Agenzia nazionale per le nuove tecnologie,
l'energia e lo sviluppo economico sostenibile

MINISTERO DELLO SVILUPPO ECONOMICO

Ricerca di Sistema elettrico

Ossi-Combustione Turbolenta di Metano in Atmosfera di CO2 Supercritica

E. Giacomazzi, D. Cecere, N. Arcidiacono, F.R. Picchia

Report RdS/PAR2017/196

OSSI-COMBUSTIONE TURBOLENTA DI METANO IN ATMOSFERA DI CO2 SUPERCRITICA

E. Giacomazzi, D. Cecere, N. Arcidiacono, F.R. Picchia (ENEA, DTE-PCU-IPSE)

Settembre 2018

Report Ricerca di Sistema Elettrico
Accordo di Programma Ministero dello Sviluppo Economico - ENEA
Piano Annuale di Realizzazione 2017
Area: Generazione di energia con basse emissioni di carbonio
Progetto B.2: Polo Tecnologico del SULCIS: Tecnologie e Metodologie "Low Carbon" e Edifici ad Energia Quasi Zero (nZEB)
Obiettivo: Parte A1 - a.2 - Cicli a CO2 supercritica
Task a.2.3 - Studi mediante simulazione numerica (HeaRT)
di processi di ossi-combustione in atmosfera di CO2 supercritica
Responsabile del Progetto: Franca Rita Picchia, ENEA

Indice

Sommario

Negli ultimi anni é cresciuto l'interesse nei cicli turbogas a CO_2 supercritica. Anche se la tecnologia di ossi-combustione alle elevate pressioni in gioco (circa 300 bar) é ancora lungi dall'essere matura, tali cicli nella loro configurazione semi-chiusa (OXYSCO2) sono molto promettenti e sono in grado di risolvere due problemi molto attuali del sistema elettrico: la flessibilitá operativa dei sistemi di generazione da fonte fossile a supporto della generazione da fonte rinnovabile non programmabile, e la riduzione delle emissioni inquinanti e climalteranti. Di fatto, i cicli s-CO_2 con ossi-combustione integrano la flessibilitá dei cicli turbogas semplici (OCGT) con un'efficienza prossima a quella dei cicli combinati (CCGT) e con una efficiente cattura della CO_2 a costo quasi zero. In sintesi, gli impianti di potenza OXYSCO2 rappresentano oggi una tecnologia emergente, la cui capacitá non é stata ancora dimostrata, anche se sono stati finanziati due importanti progetti negli Stati Uniti.

La sperimentazione alle alte pressioni in gioco puó essere proibitiva, soprattutto per l'applicazione di alcune tecniche diagnostiche, come quelle basate su laser. Gli stessi impianti da realizzare sono molto costosi. Di conseguenza, la simulazione numerica si pone come uno strumento indispensabile sia per la ricerca che per la progettazione. Occorre sottolineare che anche la simulazione numerica dell'ossi-combustione alle condizioni estreme richieste non é scontata. Esistono problemi di accuratezza modellistica (per esempio, la capacitá di catturare grandi variazioni delle proprietá quando i fluidi attraversano la pseudo-boiling line), di efficienza computazionale (equazioni di stato troppo accurate, ma complesse, non possono essere usate in approcci di simulazione giá per loro stessa natura computazionalmente molto onerosi, tipo LES e DNS), e di tipo puramente numerico (gli elevati gradienti spaziali di densitá da risolvere mettono a dura prova la robustezza e stabilitá degli schemi adottati).

Nella precedente annualitá, il codice HeaRT sviluppato da ENEA ha con successo simulato il mescolamento tra getti di diversa fase: in particolare, é stato simulato uno shear-layer temporale relativo al mescolamento turbolento a 40 bar tra un getto di azoto liquido iniettato a 118 K e 5 m/s con un getto coassiale di idrogeno gassoso a 270 K e 120 m/s. Le simulazioni hanno evidenziato la robustezza dello schema numerico $AUSM^+ - up$ selezionato ed implementato per i termini convettivi delle equazioni di trasporto. Si ricorda che nel codice HeaRT lo schema $AUSM^+ - up$ é stato accoppiato ad una procedura di interpolazione WENO (ordine 5-3) per la ricostruzione degli stati destro e sinistro delle variabili di campo, con l'ulteriore possibilitá di ricorrere ad una interpolazione meno costosa, ma anche meno accurata, quella QUICK (ordine 3). Ritenendo il test prima descritto sufficientemente impegnativo dal punto di vista numerico, si é pensato di aver risolto nel codice HeaRT il problema della corretta risoluzione di forti gradienti spaziali di densitá, soprattutto dovuti a "discontinuitá materiali o di contatto": queste discontinuitá sono quelle che si incontrano quando due fluidi con proprietá diverse (in particolare, velocitá del suono e calori specifici, in base alla nostra esperienza) sono a contatto.

Nella presente annualitá é stato inizialmente eseguito un nuovo test ancor piú impegnativo di quello descritto precedentemente: si tratta dell'iniezione transcritica (pressione superiore a quella critica, ma temperature di iniezione inferiore a quella critica) di due getti criogenici di ossigeno e metano liquidi in un ambiente riempito con una miscela di prodotti caldi di combustione a $1200\,K$ e $100\,bar$ (vedi Fig. 0.1). Questa simulazione ha messo a dura prova gli schemi numerici adottati per l'integrazione spaziale delle equazioni di trasporto. Sono stati riscontrati problemi di stabilitá sull'interfaccia tra l'ossigeno liquido ed i gas caldi, in corrispondenza quindi della transizione di fase e del massimo gradiente spaziale di densitá. I problemi riscontrati non sono stati del tutto risolti: sono state individuate delle possibili soluzioni, alcune giá in fase di test, altre ancora da implementare ed investigare. Essendo l'iniezione dei reagenti nei cicli OXYSCO2 molto probabilmente supercritica e non transcritica, si é deciso di posticipare la soluzione dei problemi di stabilitá numerica riscontrati per getti criogenici.

Visto che le temperature dell'ossi-combustione di metano possono essere elevate e sono coinvolte specie chimiche con elevato coefficiente di assorbimento radiativo, il ruolo del trasferimento radiativo di energia potrebbe essere rilevante. Occorre evidenziare che tale ruolo non é noto alle pressioni tipiche dei cicli OXYSCO2; anche gli stessi dati sui coefficienti di assorbimento sono incogniti. E' stata quindi fatta un'analisi della letteratura attuale. Sono stati raccolti ed implementati nel codice HeaRT i dati a pressione atmosferica relativi all'assorbimento medio di Planck delle specie chimiche piú importanti dal punto di vista radiativo (CO, CO_2, H_2O, CH_4). Sapendo che la pressione intensifica tali assorbimenti, si é poi deciso di effettuare un'analisi semplifi-

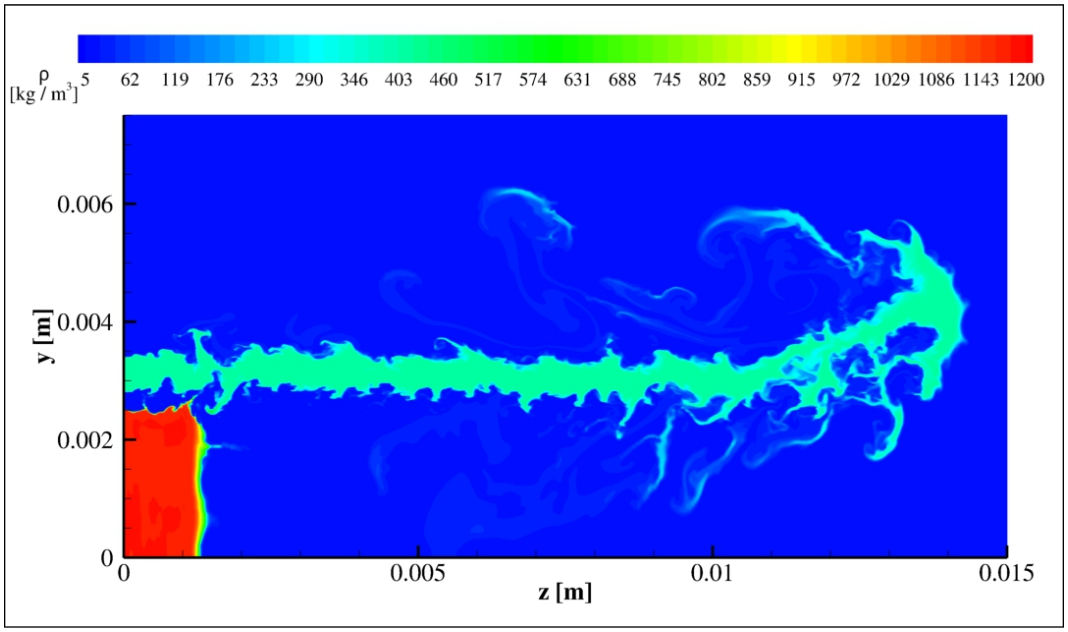

Figura 0.1: Campo istantaneo di densitá nella simulazione del mescolameto di due getti criogenici transcritici di ossigeno e metano liquidi in un ambiente riempito con prodotti caldi di combustione a 1200 K e 100 bar.

cata di tipo parametrico per investigare quello che accade alle alte pressioni: i coefficienti di Planck sono stati semplicemente intensificati tramite un fattore moltiplicativo. Parallelamente é stata iniziata una collaborazione con il gruppo del Centro di Astrofisica di Harvard che detiene un database spettroscopico ad alta risoluzione (HITRAN/HITEMP) ed é il riferimento mondiale in questo ambito. I ricercatori del centro di Harvard hanno iniziato i calcoli dei coefficienti di assorbimento spettrale delle specie chimiche piú importanti prima elencate fino a 400 bar.

Infine, é stata affrontata la simulazione di un caso di ossi-combustione a 295 bar di un getto centrale di metano a 100 m/s con uno coassiale di ossigeno a 25 m/s, iniettati in un'ulteriore corrente principale di CO_2. Tutti i flussi sono iniettati allo stato gassoso. In questa annualitá l'attenzione non é stata posta sulla strategia di iniezione dei reagenti per ottenere un efficiente mescolamento e successiva combustione. La configurazione dell'iniezione adottata é quella di un semplice shear-layer, con una piccola zona "calda" tra il getto di ossigeno e quello di metano, in cui é iniettata una miscela di prodotti di combustione ad alta temperatura e bassa velocitá per evitare problemi di ancoraggio della fiamma. Negli anni successivi occorrerá sviluppare opportune strategie di iniezione per produrre un efficiente mescolamento e studiare la stabilitá della fiamma.

Sono stati usati diversi livelli di diluizione del getto di ossidante, evidenziando, nel caso delle forti diluizioni, notevoli problemi di ancoraggio della fiamma dovuti alla grande concentrazione di CO_2; tali problemi hanno prodotto una combustione poco efficiente, caratterizzata da pacchetti reagenti (con temperature che possono essere anche molto elevate) estremamente pericolosi per una eventuale turbina a valle del combustore. Questo é sintomo di un pessimo mescolamento tra i reagenti dovuto ad una mancanza di strategia di iniezione. Le simulazioni con una bassa diluizione dell'ossigeno (10% di CO_2 in volume) evidenziano una fiamma molto frastagliata: un esempio di campo istantaneo di temperatura e di frazione massica di metano é riportato in Fig. 0.2. Anche se la cinetica chimica adottata é semplificata (un'unica reazione globale), si possono estrarre dei risultati molto interessanti. Lavorare con un getto di ossigeno poco diluito comporta temperature molto elevate, superiori ai 3000 K; anche passando a meccanismi piú dettagliati che convolgono specie radicali coinvolte in reazioni endotermiche, la mitigazione in termini di temperatura puó essere al piú di circa 300-400 gradi. Il fronte appare notevolmente corrugato, evidenziando la presenza di piccole scale, sia chimiche che fluidodinamiche (turbolente): infatti, l'elevata pressione intensifica sia la velocitá di reazione che il numero di Reynolds. Nonostante la semplificata metodologia scelta per considerare l'effeto della pressione sui coefficienti di assor-

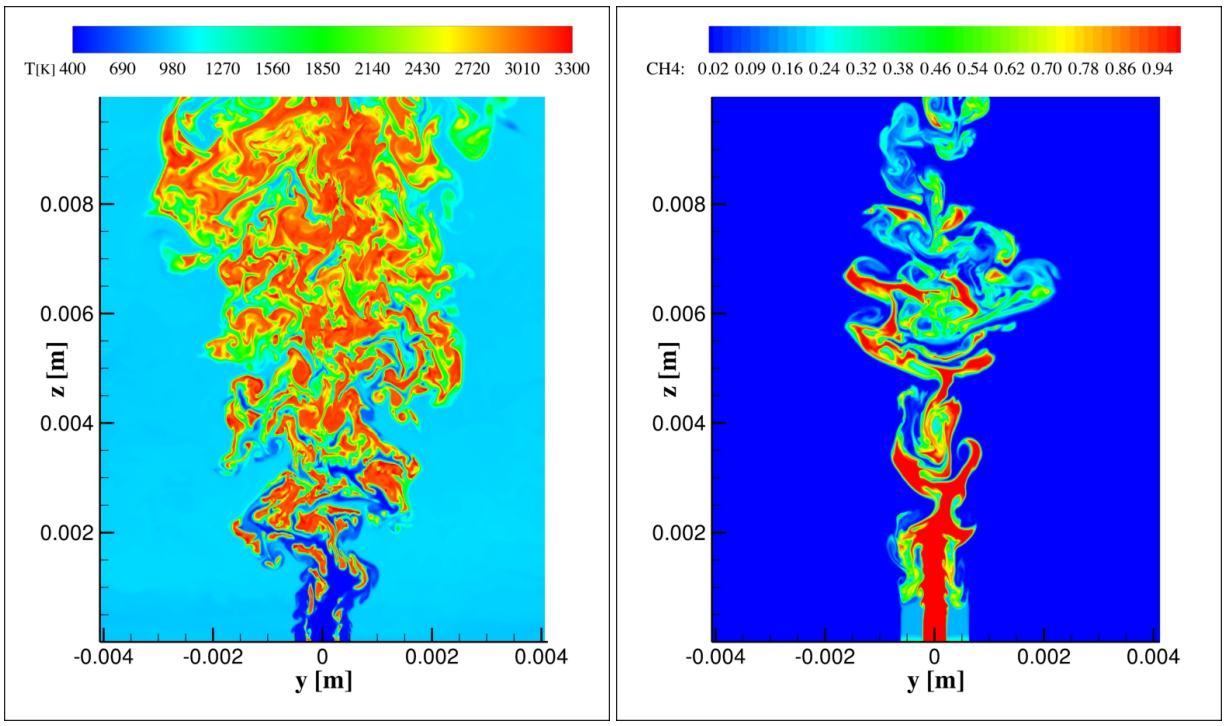

Figura 0.2: Distribuzione istantanea della temperatura e della frazione massica di metano per il caso in cui il getto di ossigeno é diluito al 10% ed in cui i coefficienti di assorbimento medi di Planck sono intensificati di un fattore 1000.

bimento delle specie chimiche (i valori atmosferici sono stati moltiplicati per 1000), il modello M1 adottato per il trasferimento dell'energia radiante é sufficientemente dettagliato da tenere in conto le diverse opacitá dei gas localmente. Il risultato piú importante ottenuto dal confronto dei budget dei termini presenti nell'equazione dell'energia totale é che l'interazione tra cinetica chimica e irraggiamento sia dominato dalla cinetica chimica: di fatto, non sono stati rilevati fenomeni di radiation cooling, e i risultati ottenuti senza e con modello radiativo sono molto simili. Questo perché, anche con una intensificazione dei coefficienti di assorbimento medio di Planck di un fattore 1000, il termine sorgente radiativa nell'equazione dell'energia é almeno tre ordini di grandezza piú piccolo di quello chimico (rilascio di calore).

In conclusione, con le notevoli migliorie apportate negli ultimi anni al codice HeaRT, questo si pone ora come uno strumento di calcolo numerico parallelo avanzato, adeguato per la simulazione fluidodinamica di flussi turbolenti, reagenti e non, in condizioni di gas reale. Un pó di lavoro sugli schemi numerici resta ancora da fare per l'entuale simulazione di getti transcritici (criogenici), in particolare di ossigeno: questi aspetti saranno affrontati nelle prossime annualitá solo se l'iniezione criogenica sará una delle possibili strategie di iniezione potenzialmente adottabili nei cicli turbogas OXYSCO2. Gli studi che verranno condotti con il codice HeaRT nelle prossime annualitá verteranno sulla definizione di una opportuna strategia di combustione e sulle modalitá di iniezione dei reagenti, per arrivare al "concept-design" della piastra di iniezione di $CH_4/O_2/S - CO_2$ e del combustore di un ciclo a CO_2 supercritica con ossi-combustione.

1 A Numerical Experiment of Transcritical Injection

In the previous year, a temporal shear-layer of liquid nitrogen and gaseous hydrogen at 40 bar was simulated to check and prove the robustness of the selected and implemented spatial numerical scheme for the convective terms of the transported equations [1].

A more difficult test is here performed to check further the stability of the numerical scheme. The numerical experiment consists in the transcritical injection (pressure higher than the critical one, but temperature below the critical one) of liquid oxygen and liquid methane and their mixing in a volume initially filled with a mixture of hot combustion products (CO, CO_2, H_2O) at 1200/, K. The liquid oxygen is injected from a central pipe (internal duct diameter 5.0 mm) at 2 m/s and at 85 K and the liquid methane is injected coaxially (internal and external duct diameters 5.6 and 6.8 mm, respectively, and wall thickness 0.3 mm) at 28 m/s and 120 K. The operating pressure is 100 bar. Based on the width of the pipes, the liquid oxygen and methane Reynolds numbers are nearly 50000 and 64000, respectively.

1.1 The Transcritical Test

In this test the density gradients are very steep: in the central oxygen stream the density is nearly 1180 $\rho\, kg/m^3$, while in the faster coaxial methane stream it is nearly 415 $\rho\, kg/m^3$; in the hot product environment density reaches values as low as $\sim 5\, kg/m^3$.

The computational domain is two-dimensional and consists of a single zone: $2.0 \times 1.5\, cm$ in the streamwise (z) and radial (y) directions, respectively, with a discretization of $1169 \times 770 = 900130$ grid nodes ($z \times y$). The inlet boundary is located on the left side of the computational domain, and it is modelled through reflecting boundary conditions: velocity, temperature, composition are specified, while pressure is extrapolated from the computational domain by means of a nil normal gradient condition. A single inlet profile for these quantities was provided to the code. The thin wall separating the two jets was modelled by imposing an inlet velocity of 1 mm/s in the corresponding spatial region. Synthetic isotropic turbulence was also forced at the inlet of the two jets, assuming a velocity fluctuation of 10% of their bulk velocity, and a streamwise length scale of $8 \cdot 10^{-5} m$ and $6 \cdot 10^{-5} m$, respectively for the oxygen and methane flows. The top boundary was modelled as a viscous wall, while the central axis as an eulerian boundary. The outlet boundary on the right of the computational domain was modelled as a partially non-reflecting boundary.

A snapshot of density field is shown in Fig. 1.1. The central high density liquid transcritical oxygen is entering the chamber. Its interface starts to exhibit some fluidynamic instabilities: some ligaments protrude towards the hot combustion products and towards the methane jet, thus promoting intense turbulent mixing. The methane jet has a more convoluted interface due to its higher Reynolds number. Since the cryogenic flows are heated by the hot mixture in the chamber, their interfaces experience a supercritical transition from the liquid to the gaseous phase. This is the complexity of such a simulation.

It is remineded that the $AUSM^+ - up$ numerical scheme was adopted for the convective terms of the transport equations, while the second order centered scheme is used for diffusive fluxes. Although suh a numerics was proved to be sufficiently robust to simulate the mixing between liquid nitrogen and gaseous hydrogen at 40 bar, it was not robust enough in the present case: the simulation diverged at some points along the oxygen interface.

The stability of the numerical scheme requires some more work, e.g., the adoption of specific spatial filters. Since in supercritical CO_2 gas turbine cycles the injection of reactants is likely to be supercritical (not in liquid phase), the furter activities on numerics to solve liquid injection is delayed.

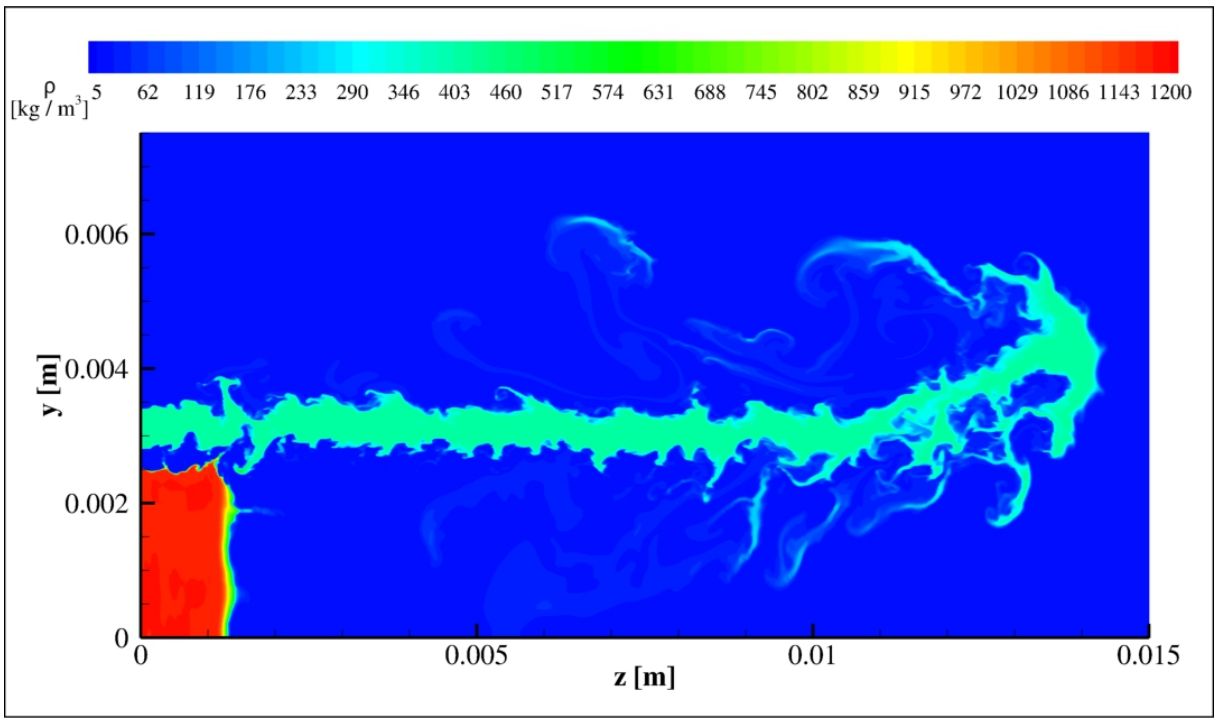

Figura 1.1: Snapshot of density field in the simulation of the turbulent mixing between two cryogenic trans-critical liquid jets of oxygen and methane in a chamber filled in with hot combustion products at 1200 K and 100 bar.

2 The Radiative Transfer of Energy

The Radiative Trasfer of Energy (RTE) is a very important mechanism in several applications: high-pressure and high-temperature engine combustion chambers, rocket propulsion, hypersonic vehicles, spacecraft atmospheric reentry, ablating thermal protection systems, glass manufacturing, plasma generators, nuclear fusion.

At industrial furnace and combustion chamber temperatures the gaseous species that absorb and emit significantly are CO_2, H_2O, CO, SO_2, NO, and CH_4. Other gases, such as N_2, O_2 and H_2, are transparent to infrared radiation and do not emit significantly; however, they become important absorbing/emitting contributors at very high temperatures. A non-negligible contribution to radiation is also providied by hot carbon (soot) particles within the flame and from suspended particulate material (as in pulverized-coal combustion).

In gases, the absorption coefficient κ_λ often varies strongly with wavelength, temperature and pressure. Emission and absorption spectra can exhibit lines and continuous regions: the lines are the result of transitions between bound energy states, while the continuos part is due to photo-dissociations, photo-ionization, free electron-atom-photon interactions. Differently from solid surfaces that can be considered opaque, gas properties exhibit very irregular wavelength dependencies: absorption or emission by gases is significant only in certain wavelength regions, especially when the gas temperature is below a few thousand Kelvin.

Emission and absorption coefficients of gases increase proportionally to the concentration of the participating species, and hence to the mixture pressure for a given species mass or molar fraction. Besides, the spectral coefficients vary with temperature but also with pressure. There are some physical mechanisms that can broaden the line (changes in in amplitude, width and shape): natural, Doppler, collision, and Stark broadening [2]. The collision broadening is the most important in engineering applications involving infrared radiation. Increasing pressure results in spectral line broadening, mainly due to molecular collisions (since the gas density increases), up to wider and more overlapping lines than at lower pressures: the result is that the gas becomes "grayer" (opaque), as shown for example in Fig. 2.1 for the absorption coefficient of a mixture containing 1% CO_2 and 2% H_2O. The absorption coefficient of cold lines decreases when the temperature increases, but towards high wavelength, hot lines appear thus resulting in a slight increase of the absorption coefficient.

When the total emission from a volume element of absorbing medium is to be calculated, the appropriate mean absorption coefficient is the Planck mean absorption coefficient, κ_P, defined as

$$\kappa_P(T,p) = \frac{\int_{\lambda=0}^{\infty} \kappa_\lambda(T,p)\, I_{b\lambda}(T)\, d\lambda}{\int_{\lambda=0}^{\infty} I_{b\lambda}(T)\, d\lambda} = \frac{\pi}{\sigma T^4} \int_{\lambda=0}^{\infty} \kappa_\lambda(T,p)\, I_{b\lambda}(T)\, d\lambda, \tag{2.1}$$

where $I_{b\lambda}(T)$ and $\kappa_\lambda(T,p)$ are the blackbody intensity and the absorption coefficient at the wavelength λ, respectively; $\sigma = 5.67 \times 10^{-8} WK^{-4}m^{-2}$ is the Stefan-Boltzmann constant. The κ_P is the mean of the spectral coefficient weighted by the blackbody (Planck distribution) emission spectrum. The Planck mean is convenient since it depends only the local properties and it can be tabulated.

Values for κ_P have been estimated in the past [5, p. 253-324], but these are today known to be seriously in error, especially at higher temperatures and pressures. Today, the Planck mean absorption coefficient for single species can be calculated [6] directly from high-resolution spectroscopic databases such as HITRAN [7] and HITEMP [8]: the new databases, with the inclusion of more lines from higher vibrational energy levels provide more accurate absorption data, thus resulting in κ_P at high temperature generally larger than those obtained through older databases. Based on spectral line information for different radiating species, since absorption coefficients are additive, κ_P consists of individual contributions from all spectral lines, i.e.,

$$\kappa_P(T,p) = \frac{\pi}{\sigma T^4} \sum_i \int_{\lambda=0}^{\infty} \kappa_{\lambda_i} I_{b\lambda} d\lambda = \frac{\pi}{\sigma T^4} \sum_i I_{b\lambda_i} \int_{\lambda=0}^{\infty} \kappa_{\lambda_i} d\lambda = \sum_i \frac{\pi I_{b\lambda_i}(T)}{\sigma T^4} \mathcal{S}_i(T,p) \tag{2.2}$$

where the sum is over all the spectral lines and $\kappa_{\lambda_i}(T,p)$ is the absorption coefficient due to the $i-th$ spectral line centered at λ_i, and $\mathcal{S}_i$ is the line-integrated absorption coefficient or line strength (that is listed in the HITRAN and HITEMP databases). In deriving Eqn. (2.2) the Planck function has been assumed constant for each single line contribution since it varies little across each spectral line.

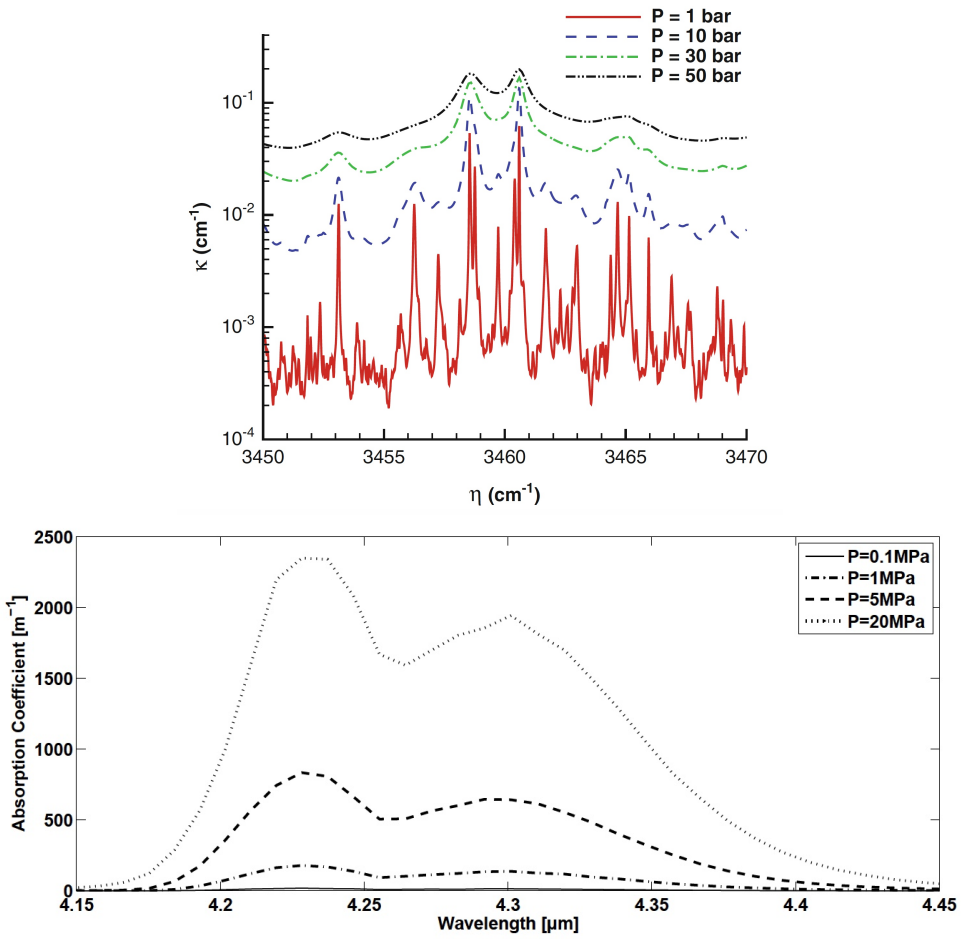

Figura 2.1: (Top) Wide band absorption coefficient spectra of a mixture containing 1% CO_2 and 2% H_2O [3, p. 138]; (bottom) narrow band absorption coefficient spectra of pure CO_2 at 600 K for different pressures [4].

Looking at available literature, some interesting results are here reported. Numerical simulations of the heat transfer from the hot wall of a pipe containing a flow of CO_2 [4] showed that the influence of radiation on the flow temperature and velocity distribution decreases with an increase of the operating pressure and becomes negligible above 200 bar. This means that the radiant transfer of energy becomes weak at very high pressure since the optical thickness increases and radiation is absorbed in a very thin layer; for the problem investigated in [4], this layer is near the hot inner surface of the pipe. However, the present authors note that such conclusions should be confirmed by analysing the competition between thermal radiation and conductivity to identify the most effective heat transfer mechanism in the thin layer close to the wall, e.g., by looking at the associated budgets in the energy transport equation as done in this work.

Concerning flames, it is well known that neglecting radiation at atmospheric pressure conditions may lead to overprediction of temperature of up to 200 K. However, it has to be noted that numerical predictions strongly depend on the RTE model adopted: the usually-employed optically-thin or gray radiation models lead to underprediction of temperature of up to 100 K and more [9, 10]. Furthermore, radiation is enhanced by turbulence through strong nonlinear interactions between temperature and radiative property fluctuations (TRI): such interactions increase the heat loss from a flame leading to a reduction in the local gas temperature of 200 K and more. The TRI cooling effect is even enhanced in high-pressure combustors that typically exhibit larger optical thicknesses [11, 12]. For systems where RTE is important, radiation was shown to be equivalent to a large nonlinear diffusion term: in fact, the radiant transfer of heat can work as a preheating mechanism as conduction of heat, thus resulting in higher flame speeds [13].

Focusing on peak flame temperature, radiation typically reduces it in low pressure flames. Although radiation

effects become more pronounced as the pressure is increased (due to increased emission/absorption), the peak flame temperature is less affected by radiation because of the faster chemical reactions, as also observed in [3, p. 139]. In fact, according to the Arrhenius law, the chemical reaction rate is proportional to reactant molar concentrations raised to a power that is equal to the number of moles that have to collide for the reaction to occur. Hence, the reaction rate is proportional to p for first-order reactions and to p^2 for second-order reactions; three-body reactions, are even more enhanced [14].

2.1 The $M1$ Radiant Transfer of Energy Model

In the simulation presented in the next Chapter, the radiant transfer of energy is taken into account by means of the M_1 diffusive model briefly described in the following. For the time being, turbulence-radiation interaction is neglected, although it is expected to play an important role in flame cooling at the high-pressure conditions of the present simulations. Another simplification is the adoption of the individual species' Planck mean absorption coefficients typically used at atmospheric pressure. Since they are expected to increase by increasing pressure, the effect of multiplying them by 1000 is investigated. In the future they will be accurately calculated by using the high-resolution spectroscopic databases HITRAN [7] and HITEMP [8].

The the M_1 model, also called the maximum entropy closure radiation model, is a macroscopic radiation model. Since 1978 this model has been developed by many authors [15, 16, 17, 18, 19, 20, 21]. This model is based on field equations for the radiative energy and the radiative heat flux vector. The limit is that it is valid for non scattering media. The main advantage is that it is independent of the opacity of the media, i.e., it adapts itself and works from thin to thick optical thickness. An averaged form of the M_1 model for turbulent flows also exists [22, 23], even though very complex and expensive to solve. A simplified formulation of this model was finally developed [24]: this is better suited for combustion problems and thus applied in present simulations.

When the medium follows a Rayleigh law, the M_1 model consists of a transport equation for the radiant energy density, E_r, (units are $J\,m^{-3}$) i.e.,

$$\frac{\partial E_r}{\partial t} + \nabla \cdot \boldsymbol{F}_r = c\left(\sigma_p a T^4 - \sigma_E E_r\right) , \tag{2.3}$$

and a transport equation for its flux vector, $\boldsymbol{F}_r$, (units are $J\,m^{-2}\,s^{-1}$) i.e.,

$$\frac{1}{c}\frac{\partial \boldsymbol{F}_r}{\partial t} + c\,\nabla \cdot (\boldsymbol{D}_r E_r) = -\sigma_F \boldsymbol{F}_r , \tag{2.4}$$

where T is the temperature, $c = 299792458\,ms^{-1}$ is the speed of light, $a = 4\,\sigma_{SB}/c = 7.565767{\cdot}10^{-16}\,J\,m^{-3}\,K^{-4}$, $\sigma_{SB} = 5.6704{\cdot}10^{-8}\,J\,m^{-2}\,s^{-1}\,K^{-4}$ being the Stefan-Boltzmann constant, σ_P is the Planck mean absorption coefficient of the mixture, σ_E and σ_F its two effective absorption coefficients, $\boldsymbol{D}_r$ the nondimensional Eddington tensor that takes into account the local opacity of the flame.

The previous equations are very stiff and difficult to solve. A more friendly form can be obtained assuming that radiative energy rapidly reaches its equilibrium state, i.e., neglecting the time derivatives in Eqns. (2.3) and (2.4). In this way two diffusion equations are obtained:

$$\nabla \cdot \left[\frac{1}{\sigma_F}\nabla \cdot (\boldsymbol{D}_r E_r)\right] = -\left(\sigma_P a T^4 - \sigma_E E_r\right) \tag{2.5}$$

and

$$-\nabla \cdot \left[\frac{\boldsymbol{D}_r}{\sigma_E}\nabla \cdot \boldsymbol{F}_r\right] + \sigma_F \boldsymbol{F}_r = -c\nabla \cdot \left[\frac{\sigma_P}{\sigma_E}\boldsymbol{D}_r a T^4\right] . \tag{2.6}$$

It is observed that in the present numerical experiment, since it deals with oxy-combustion in a supercritical CO_2 atmosphere and since the CO_2 becomes optically thick by increasing pressure, the radiation transport can be correctly modelled by a diffusion process.

The quasi-steady radiative transfer equations are solved (by using a SOR technique coupled to a median spatial filter) periodically at some time steps to update the radiative sink/source term, $\dot{S}_{rad} = -\nabla \cdot \boldsymbol{F}_r \left[W/m^3\right]$, in the transported energy equation.

3 A Numerical Experiment of Supercritical Injection and Oxy-Combustion

In the recent years it is growing the interest on s-CO_2 power cycles equipped with oxy-combustion as a new technology able to solve simultaneously all the above issues, integrating the OCGTs typical operational flexibility with an efficiency target closer to CCGTs and with both flexible and efficient carbon capture capabilities. Oxy-combustion s-CO_2 (OXYSCO2) power plants are internal combustion engines using s-$CO2$ as working fluid, conceptually similar to conventional gas turbines. As an emerging technology, the OXYSCO2 engine capabilities are not yet demonstrated, although there are on-track two important research project in US. Concerning their operational flexibility, it is likely that the heat exchangers will be the most important barrier at plant component level and combustion dynamics at process level. Combustion dynamics knowledge related to conventional gas turbines can lead to a basic understanding of the relationships between the engine operational flexibility and combustion dynamics. However, the strong differences in thermo-physical properties between the perfect gas model and the supercritical fluid model require a complete re-shaping of the combustion modelling strategies as well as new customized numerical tools.

Oxy-combustors of s-CO_2 gas turbines are being designed to operate at 300 bar. Experimental work at such high-pressure conditions may be prohibitive: the use of advanced laser diagnostics is not an easy task to achieve, and very few examples exist in literature; besides, facilities themselves may be very expensive. Hence, most of research and design in this area is based on numerical simulation. However, also the numerical approach is not an easy task, suffering problems of both modelling accuracy (e.g., the ability to capture huge variations of fluid properties when crossing the pseudo-boiling line) and computational efficiency (too complex and accurate equations of state cannot be used in time-consuming simulations, like LES and DNS). Furthermore, numerical schemes are stressed hardly: the high-density gradients typical of some applications (as those involving liquid injection) and the multi-species transport enhance wiggle formation in fully compressible solvers.

The aim of this Chapter is to investigate turbulent non-premixed methane oxy-combustion in an atmosphere rich in CO_2 at supercritical conditions by means of Large Eddy Simulation. A simple shear-layer configuration typical of slot burners is considered: the fuel is CH_4 and flows through the central slot, the oxidant O_2/CO_2 (90, 30, 10% O_2 by mass) mixture flows on both sides of the slot, and a pilot flame is imposed at the inlet between the two streams of reactants to force ignition.

Fully compressible Navier-Stokes equations coupled to the Peng-Robinson cubic equation of state for real gases in its improved translated volume formulation are solved adopting the Large Eddy Simulation approach. The dynamic Smagorinsky and the LTSM subgrid scale models are used for turbulence and combustion closures. Among the diffusive mechanisms only the Dufour effect is neglected; transport properties are accurately calculated. The M_1 radiant transfer of energy model is adopted without considering turbulence-radiation interactions.

Numerical results are examined to highlight different physical aspects of the flow: the effect of oxygen stream dilution on the flame anchoring and topology; the effect of the radiant transfer of energy on the flame structure; diffusive mechanisms, to identify the fastest processes through the comparison of characteristic times.

3.1 Physical and Numerical Models

In this work the compressible Navier-Stokes equations are solved for a reacting real gas flow at supercritical conditions for which the Peng-Robinson cubic equation of state in its improved volume translated formulation is assumed.

The mathematical models adopted are derived for a fluid of N_s chemical species. The constitutive laws assumed to describe the behaviour of the fluid are here reported. They simply model the microscopic molecular diffusion of momentum, energy and mass, i.e., they model the momentum flux $\boldsymbol{S}$, the heat flux $\boldsymbol{Q}$ and the species mass flux $\boldsymbol{J_i}$.

A Newtonian fluid is considered and the Stokes' assumption is made: it is characterized by the following constitutive relation between the stress, $\boldsymbol{S}$, and the strain rate, $\boldsymbol{E}$,

$$\boldsymbol{S} = -\left(p + 2/3\,\mu\nabla\cdot\boldsymbol{u}\right)\boldsymbol{I} + 2\mu\boldsymbol{E} = -p\boldsymbol{I} + \boldsymbol{\mathcal{T}}\ , \tag{3.1}$$

μ being the viscosity; $\boldsymbol{\mathcal{T}}$ is the viscous part of the stress tensor.

The mass diffusion flux has three contributions [25]. The first one is due to concentration gradients (here modelled through the Hirschfelder and Curtiss' law for multi-component mixtures) [26], the second due to pressure gradients (the baro-diffusion mechanism) [27], and the third one due to temperature gradients (the thermo-diffusion or Soret effect) [28]:

$$\boldsymbol{J}_i = \rho Y_i \boldsymbol{V}_i = \boldsymbol{J}_i^{HC} + \boldsymbol{J}_i^{BD} + \boldsymbol{J}_i^{S} = -\rho Y_i D_i \left[\frac{\nabla X_i}{X_i} + \frac{X_i - Y_i}{X_i}\frac{\nabla p}{p}\right] - \mathcal{D}_i^T \frac{\nabla T}{T}. \tag{3.2}$$

The diffusion coefficient D_i is an effective diffusion coefficient of the i-th species into the mixture (mixture-average assumption).

The thermo-diffusion, or Soret effect, is the mass diffusion due to temperature gradients, driving light species towards hot regions of the flow [29, 30]. This effect, often neglected, is neverthless known to be important, in particular for hydrogen combustion, and in general when very light species play an important role [31, 32].

Keeping apart the radiative heat transfer of energy, the heat flux has three contributions too. The first due to temperature gradients (the Fourier diffusion), the second due to mass diffusion fluxes, and the third one is the Dufour effect (reciprocal of the Soret effect):

$$\boldsymbol{Q} = \boldsymbol{q}_F + \boldsymbol{q}_{V_i} + \boldsymbol{q}_D = -K\nabla T + \rho \sum_{i=1}^{N_s} h_{s_i} Y_i \boldsymbol{V_i} + \boldsymbol{q}_D. \tag{3.3}$$

Note that this is the heat flux expression entering into the energy transport equation where formation energies are isolated in a source term, i.e., not included in the energy definition. Usually the Dufour effect (the third term) is negligible even when thermo-diffusion is not [28, p. 768] and hence it is neglected in the present work.

Molecular transport properties for individual species are accurately modelled through NIST models [33] for viscosity and thermal conductivity. The diffusion coefficient D_i of the i-th species into the rest of mixture is modelled according to the Hirschfelder and Curtiss expression [26], where the required binary diffusion coefficient is calculated by means of kinetic theory. The thermo-diffusion coefficient $\mathcal{D}_i^T$ is estimated by means of the EGLIB routines [34].

A simplified chemical mechanism consisting of 4 reactions and 6 species developed for oxy-combustion is adopted [35, Table 2]. Since main radical species are not included in the mechanism, temperature is overestimated by more than 300 K [36]. This is a first step before facing a more complex kinetics.

The transport equations are solved in the framework of Large Eddy Simulation. Unclosed turbulent combustion subgrid terms of the filtered compressible Navier-Stokes equations are modelled through the dynamic Smagorinsky model and the authors' LTSM (Localised Turbulent Scale Model) [37] turbulent combustion model.

The radiant transfer of energy is also taken into account by means of the M_1 diffusive model previously described. For the time being, turbulence-radiation interaction is neglected.

3.2 Numerical Schemes and Boundary Conditions

The numerical simulations are performed by means of the in-house parallel code HeaRT and ENEA's supercomputing facility CRESCO [38]. The HeaRT code solves the compressible Navier-Stokes equations discretised through staggered finite-difference schemes. A second-order accurate centered scheme is adopted for diffusive fluxes; convective terms are modelled through the $AUSM^{+}$-up method [39] coupled with a third/fifth-order accurate $WENO$ interpolation to reduce spurious oscillations (strongly experienced using centered schemes in high-pressure tests); such numerical spatial scheme was extensively tested by the present authors proving

its robustness and accuracy [40]. The low-storage third-order accurate Runge-Kutta method of Shu-Osher is used for time integration. The total energy is defined as sum of internal (thermal) and kinetic energy only. The authors found this choice mandatory [41, 42] to avoid, or at least reduce, unphysical energy and temperature oscillations, mainly driving to the divergence of calculation. No spurious waves were experienced in previous simulations of premixed flames, when the total energy was defined including the chemical formation contribution.

Non-reflecting boundary conditions [43, 44, 45] are implemented at open boundaries in their extended form to take into account the effect of variable transport properties [46], local heat release [47] and real gas effects [48]. It is observed that in previous and present real gas simulations the authors had to impose a higher value of the relaxation constant in the partially non-reflecting treatment of the outlet with respect to the ideal gas theoretical value (1.5 against 0.27) [43, 49] to avoid unphysical pressure drift in the whole computational domain. A synthetic turbulence generator is adopted at flow inlets [50].

3.3 The Numerical Experiment and Its Set-Up

The numerical experiment here simulated has a nominal pressure around 300 bar and consists in a simple shear-layer configuration that can be encountered in slot burners; the flow is confined by means of two no-slip adiabatic walls (at left and right of the domain). At the bottom of the computational domain there is the inlet, while the outlet is located at the top. In this preliminary work, simulations are perfomed in a two-dimensional framework to reduce computational time. The domain $y \times z$ is $8 \times 10\,mm$ and is discretised by means of 396×700 nodes. The computational nodes are uniformly distributed along the streamwise direction z, with $\Delta z \sim 1.42 \cdot 10^{-5}\,m$, and stretched from the center towards the sides along the transversal direction y, with $\Delta y_{min} \sim 8.8 \cdot 10^{-6}\,m$ and $\Delta y_{max} \sim 5.74 \cdot 10^{-5}\,m$; the aspect ratio $\Delta z/\Delta y$ is in the range $[0.25, 1.61]$.

The fuel is CH_4 and is injected centrally at $50\,m/s$ and $388\,K$; its width is $4 \cdot 10^{-4}\,m$. The oxidant O_2/CO_2 mixture flows on both sides of the methane, and a pilot flame is imposed at the inlet between the two streams of reactants to force ignition. Each oxidant jet flows at $100\,m/s$ and $450\,K$; their width is $1.95 \cdot 10^{-4}\,m$. The pilot flames imposed at the inlet exhibit a temperature distribution ranging from 900 to 2049 K and a coherent distribution of chemical species; such data come from separate calculations previously performed; these hot gases flow at $5\,m/s$ and are $10^{-4}\,m$ widen. Adjacent to each of the oxidant streams, there is a coflowing stream of CO_2 at $50\,m/s$ and $973\,K$. The (isotropic) turbulence characteristics of the jets are specified in terms of velocity fluctuations and auto-correlation length-scales: $u' = 5\,m/s$ and $l_y = 3 \cdot 10^{-5}\,m$ for the methane jet; $u' = 1\,m/s$ and $l_y = 5 \cdot 10^{-5}\,m$ for the pilot flames; $u' = 10\,m/s$ and $l_y = 5 \cdot 10^{-5}\,m$ for the oxidant jets; $u' = 5\,m/s$ and l_y ranging from 2 to $6 \cdot 10^{-5}\,m$ for the CO_2 coflowing streams. The methane jet Reynolds number (based on its bulk velocity and diameter) is nearly 142500 while its turbulent counterpart (based on the imposed velocity fluctuation and length-scale) is around 1070. The oxidant jet Reynolds number is nearly 141500, while its turbulent counterpart is around 3600 for the 90% O_2 condition; inceasing dilution with CO_2 results in higher values. The smallest dissipative scale expected comes from the Re^t_{Ox} and is nearly $10^{-7}\,m$.

Three compositions of the oxidant mixture are investigated, 90, 30 and 10% of O_2 by mass. The less diluted condition is simulated firstly without considering the radiant transfer of energy (case $NO\text{-}RTE$), then switching on the M_1 model with two different levels of absorption: in the case named $1 \times \kappa_P$ the individual species Planck mean absorption coefficients used at atmospheric pressure are adopted, while in the case $10^3 \times \kappa_P$ they are intensified by a factor 10^3. The 30% O_2 case is simulated only at the intensified condition $10^3 \times \kappa_P$. The most diluted case, 10% O_2, is simulated without the RTE model and with a wider pilot flame at the inlet, necessary to force ignition.

It is observed that the present simulations are aimed at better understanding the physics of methane oxy-combustion in a s-CO_2 environment: no particular strategies are adopted to enhance injection of reactants from the point of view of mixing. With the simple shear-layer configuration chosen, the 30% O_2 case with a small pilot flame results in no ignition of the mixture apart from some small flame pockets released downstream from the forced anchoring regions, rapidly quenched by the high aerodinamic stretching. The 10% O_2 case with a wider pilot flame results in more and larger reacting pockets characterizing a not efficient combustion (see Fig. 3.1): this happens for both $NO\text{-}RTE$ and $10^3 \times \kappa_P$ cases. These results higlight that future studies

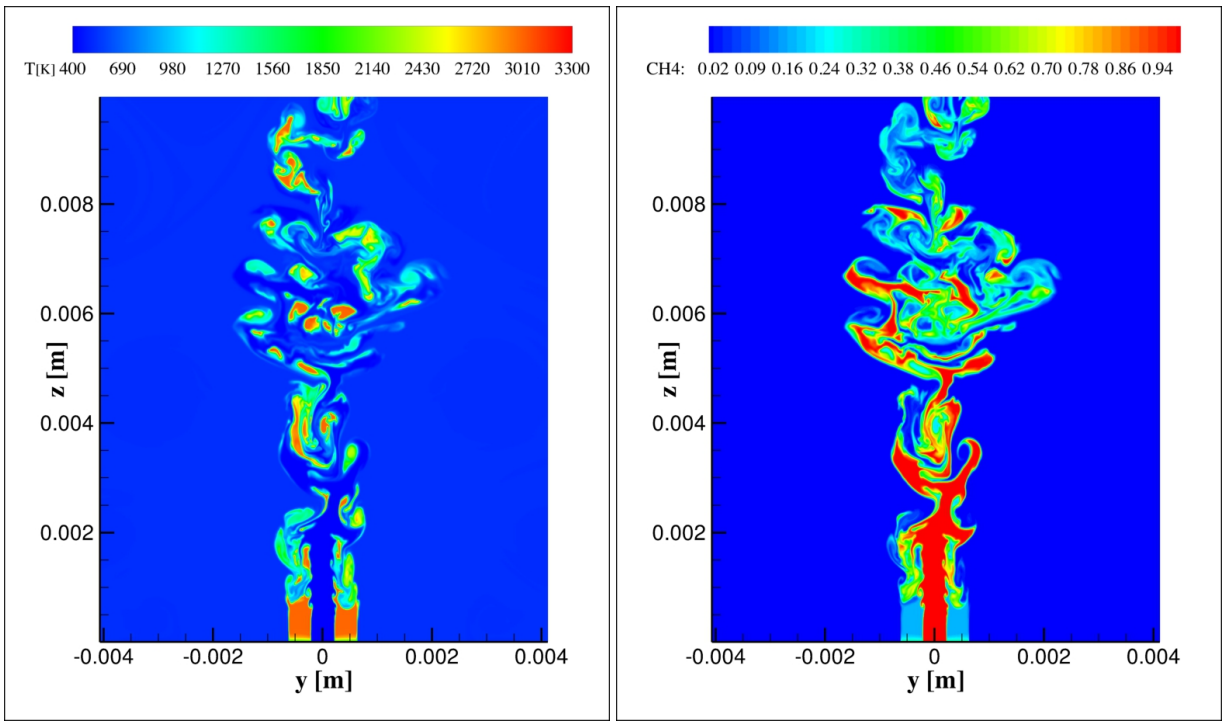

Figura 3.1: Case 10% O_2, $10^3 \times \kappa_P$, with a forced wide pilot flame. Instantaneous distribution of temperature and methane mass fraction.

should be focused on injection strategies to ensure efficient combustion with diluted oxygen streams, at least 30% by volume as imposed primarily by safety reasons in power plants [51]. Hence, since stable and efficient combustion has been achieved only in the 90% O_2 by mass case (corresponding to nearly 92% by volume), in the following the attention will be focused on the analysis of this case.

3.4 The Effect of Radiant Transfer of Energy and Flame Structure

As already stated, only the results obtained for the lowest dilution level of the oxygen stream, i.e., 90% O_2 by mass, will be analysed in detail since it is the only condition resulting in a stably anchored flame. Radiation effects were examined by performing three simulations related to the three cases *NO-RTE*, $1 \times \kappa_P$ and $10^3 \times \kappa_P$.

Comparing results obtained without considering the RTE model with those obtained using different intensification factors of the Planck mean absorption coefficients, very little differences appear in the flame structure. This happens despite the large differences in the radiation source/sink term of the energy transport equation shown in Fig. 3.2 (left). This behaviour can be easily understood by comparing the energy budgets of the different terms contributing to the total energy transport and shown in Fig. 3.2 (right). The order of magnitude of the work done by the gravity force is $10^5\ W/m^3$; the viscous work is of the order of $10^8\ W/m^3$; since they are order of magnitudes lower than the other terms, they are not shown. Then, in the ordered list of budgets there is the radiative source term with $10^{10}\ W/m^3$, followed by the heat diffusion term with $10^{11}\ W/m^3$. It can be concluded that in the present simulation the effect of radiant transfer of energy is negligible even with the intensifying factor 10^3 for the κ_P. However, accurate calculation of the Planck mean absorption coefficients from high-resolution spectroscopic databases is necessary to really understand if the intensification factor 10^3 here adopted is justifiable, sufficient or not. Besides this, it is reminded that turbulence/radiation interaction has not been taken into account in this work, although its contribution is expected to be enhanced in high-pressure combustors.

It is observed that the distribution in Fig. 3.2 (left) does not nearly change by substituting the radiant energy density with temperature in the abscissa, i.e., high values of E_R corresponds to high values of T. Hence, radiation cooling is active in the hottest regions of the flame but it produces a negligible effect, i.e., peak

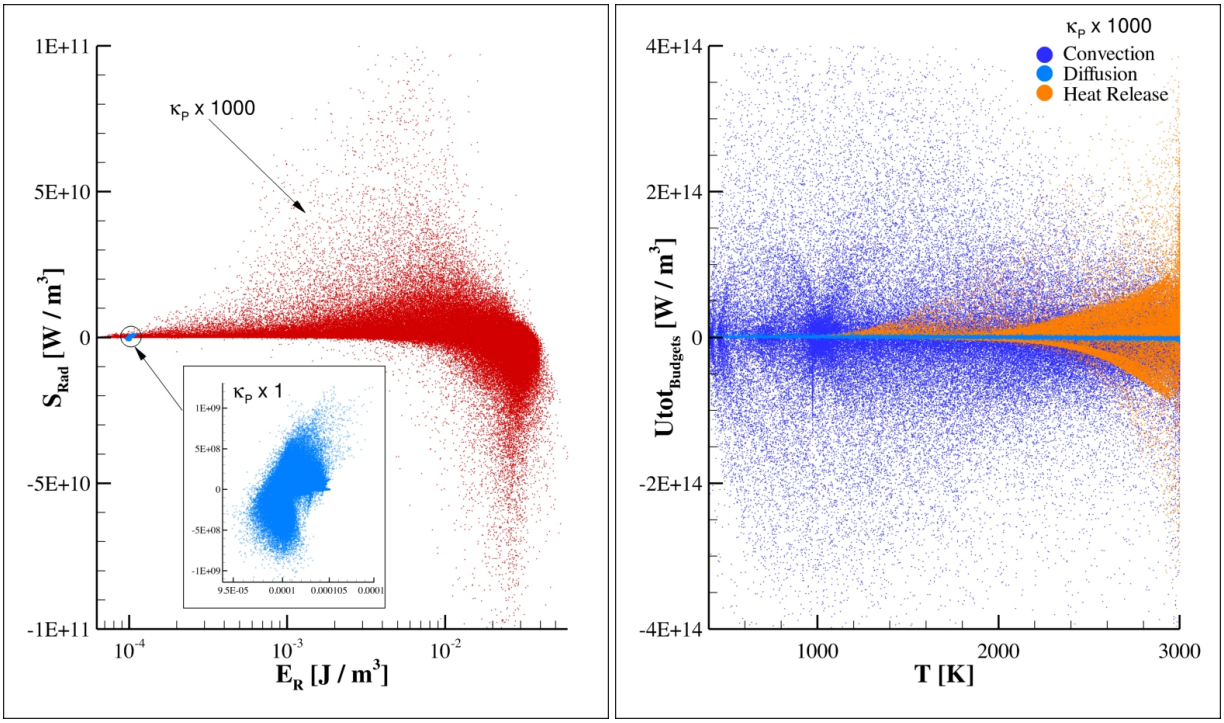

Figura 3.2: Case 90% O_2. Instantaneous distributions of the radiative source term in the total energy transport equation versus the radiant energy density for two intensifying factors of the Planck mean absorption coefficient κ_P (left). Instantaneous distributions of energy budgets related to convection, diffusion and heat release terms contributing to the total energy transport equation (right); contributions from viscous and gravity force works are lower and hence not reported.

temperatures do not decrease due to radiation transport. As a matter of fact, the competition between the enhanced radiative cooling expected and the enhanced chemical kinetics (both due to the high pressure) is here dominated by chemistry. This result is in agreement with what already observed in [3, p. 139] for high-pressure flames in air. This behaviour is here understood by noting that the heat release budget in the energy transport equation is four order of magnitudes greater than the radiative budget, as shown in Fig. 3.2. Instantaneous distributions of the radiative energy density and of the source term in the total energy transport equation for the case $10^3 \times \kappa_P$ are shown in Fig. 3.4. In particular, the radiative source/sink term is localized in thin layers. Although not shown, the results evidenced that radiative cooling (associated to negative values of S_{rad}) in this flame is limited to a very thin layer localized around the stoichiometric mixture fraction and it is more frequent in the hot products side ($\mathcal{Z} < \mathcal{Z}_{st}$).

Once clarified that in the present simulations the effect of radiation is negligible, let's examine the structure of the flame. The flame is stably anchored, showing small reacting pockets mainly aligned in the streamwise direction close to the injection, and evolving into larger scale reacting regions moving downstream, as revealed by the temperature snapshot in Fig. 3.3 (left). The reacting structures are thinner than those typically encountered at lower pressures: this is due to the accelerated chemical kinetics promoted by the high-pressure condition. The methane distribution associated to the same instant is reported in Fig. 3.3 (right) showing that the jet is corrugated by turbulence without exhibiting any laminar region on its boundaries. High-momentum O_2 ligaments penetrate the methane jet as well as CH_4 fingers also develop into the coflowing stream, thus producing isles of fuels later developing in reacting pockets.

3.5 Standard and Effective Diffusion Times and Characteristic Numbers

The attention is now focused on diffusion terms only of the Navier-Stokes equations. Characteristic diffusion times may appear when non-dimensionalising Navier-Stokes equations: the momentum diffusion (viscous)

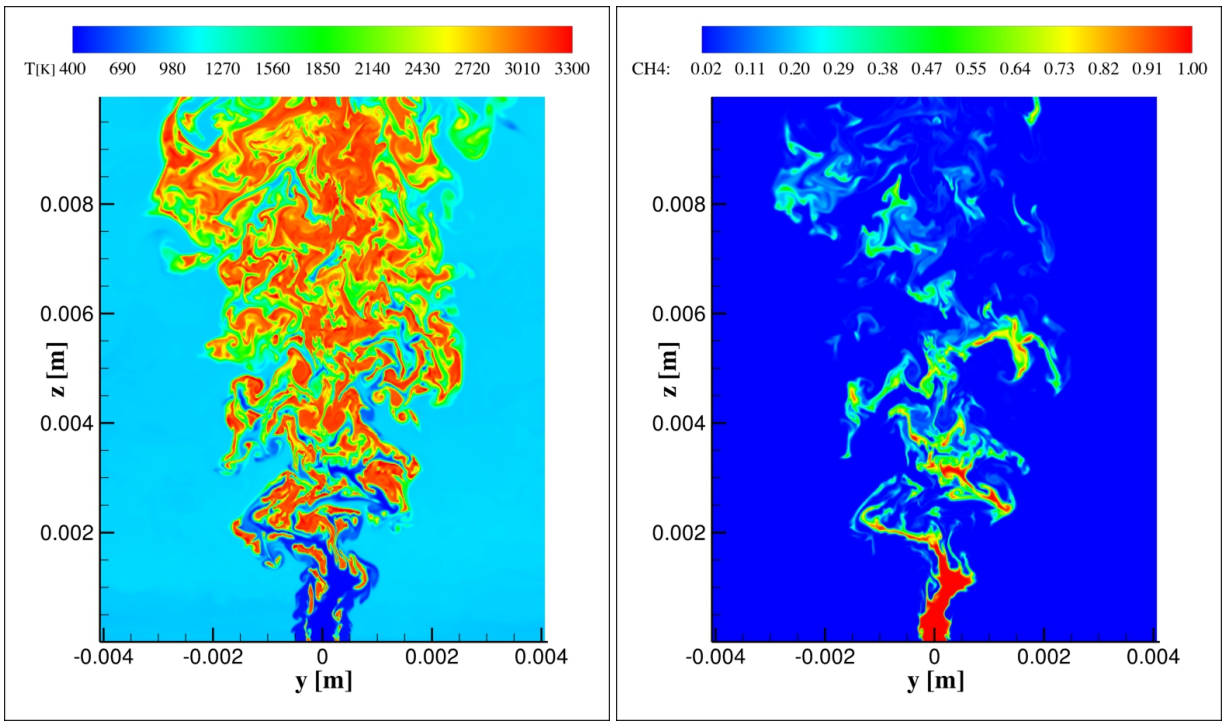

Figura 3.3: Case 90% O_2, $10^3 \times \kappa_P$. Instantaneous distribution of temperature and CH_4 mass fraction.

time $\tau_\nu = \delta^2/\nu$ (δ being a reference length scale, ν the kinematic viscosity), the mass diffusion time $\tau_{D_i} = \delta^2/D_i$ (D_i being the diffusion coefficient of the i-th species into the rest of mixture), the heat diffusion time $\tau_\alpha = \delta^2/\alpha$ ($\alpha = \kappa/\left(\rho\, C_p\right)$ being the thermal diffusivity, with κ the thermal conductivity, ρ the density and C_p the specific heat at constant pressure). The related non-dimensional numbers are: the Reynolds number Re, defined as the ratio between the momentum diffusion and convective times (the convective time being $\tau_c = \delta/U$ with U a reference velocity), the Schmidt number Sc_i, defined as the ratio between the mass and momentum diffusion times, the Prandtl number Pr, defined as the ratio between the heat and momentum diffusion times, the Lewis number Le_i, defined as the ratio between the mass and heat diffusion times.

Non-dimensional parameters can give a quick information about the relative importance of physical mechanisms. For example, the deviation of the Lewis number from unity is commonly accepted to well represent the unbalanced influence of thermal to mass diffusion. Especially for modelling purposes, some authors addressed the need to define an effective Lewis number [52, 53]. Authors in [54] observed that, not only the calculation of Le may be biased by steep gradients, but also its meaning may be questioned due to the off-diagonal terms of the diffusive transport matrix (Soret, Dufour, ...).

In [41, 42] a method to calculate effective characteristic times (and then the related non-dimensional numbers) from the Navier-Stokes equations terms was suggested. In particular, the local momentum diffusion (or viscous) time is modelled as

$$\tau_{\mathcal{T}} \sim \rho \frac{|\nabla \boldsymbol{u}|}{|\boldsymbol{\mathcal{T}}|}\Delta^2, \tag{3.4}$$

the local heat diffusion time as

$$\tau_{\mathcal{Q}} \sim \rho \frac{|\nabla h_s|}{|\boldsymbol{\mathcal{Q}}|}\Delta^2, \tag{3.5}$$

where h_s is the sensible enthalpy, and the mass diffusion time as

$$\tau_{J_i} \sim \rho \frac{|\nabla Y_i|}{|\boldsymbol{J}_i|}\Delta^2. \tag{3.6}$$

It is reminded that the module of a generic tensor $\boldsymbol{A}$ is defined as $|\boldsymbol{A}| = \sqrt{2\,\boldsymbol{A} : \boldsymbol{A}} = \sqrt{2\,A_{ij}A_{ij}}$. It is also observed that with the above expressions, the standard viscous time definition τ_ν is recovered for a non-compressible

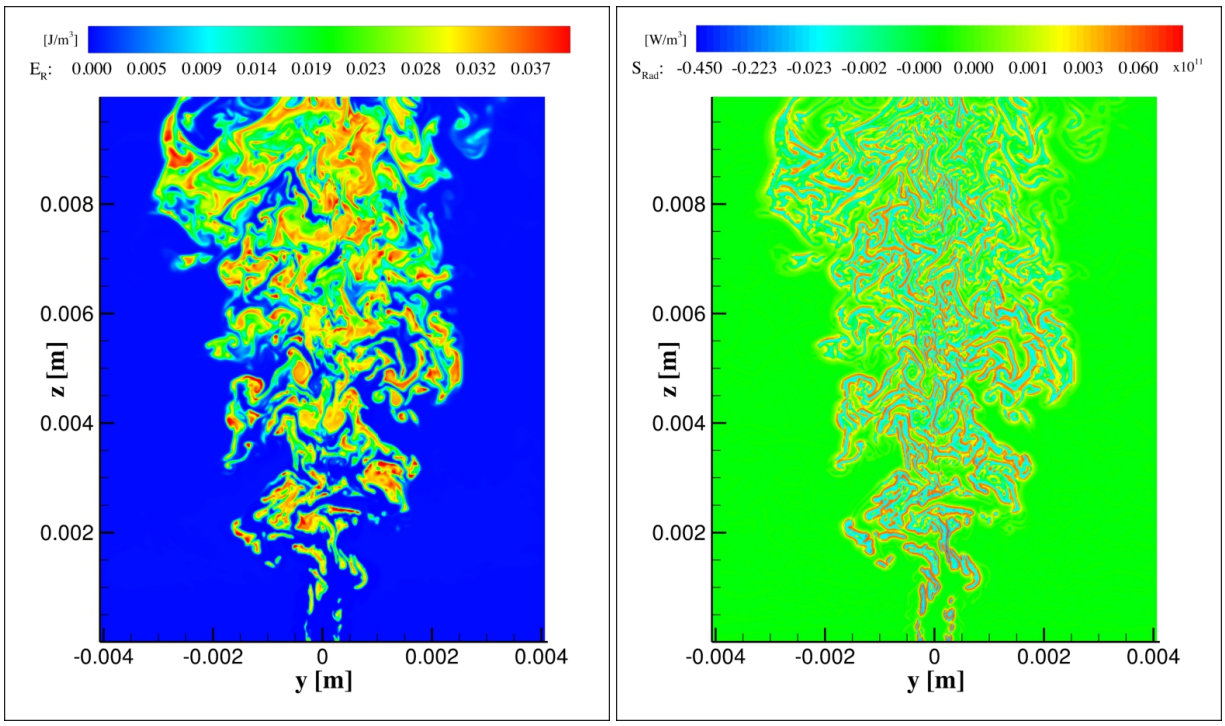

Figura 3.4: Case 90% O_2, $10^3 \times \kappa_P$. Instantaneous distributions of the radiative energy density and of the source term in the total energy transport equation.

flow; the standard heat diffusion time definition τ_α is recovered if the heat flux is limited to the Fourier contribution only; the standard mass diffusion time definition τ_{D_i} is recovered if the mass flux is limited to the Fick law only.

Effective diffusion time distributions are reported in Fig. 3.5 (left). The hydrogen is selected as the most appropriate species to evaluate the mass diffusion time, due to its low mass. Comparing the three diffusion times, it is deduced that the hydrogen mass diffusive mechanism is the fastest, followed by the heat and momentum diffusion. It is also observed that there is an overlapping region, and in particular heat and H_2 mass diffusion mechanisms can interact. Among the different mechanisms contributing to H_2 mass diffusion, the most important is that related to the Hirschfelder-Curtiss law, as shown in Fig. 3.5 (right). The Soret effect can be as fast as it at intermediate temperatures, while the baro-diffusion can be neglected.

Through the effective diffusion times, effective characteristic numbers can be evaluated and compared to their standard counterpart. Figure 3.6 shows the instantaneous distributions of the hydrogen Schmidt number: the effective and standard distributions look very similar, although the effective one is spread over the standard one. Instead, the effective Lewis number shows higher values than the standard one, especially in the high temperature regions, as reported in Fig. 3.7 (left). Similar results were found in [41, 42, 54]. Being $Le = Sc/Pr$, and since the Prandtl number distribution shown in the same figure (right) reveals effective values lower than the standard ones, it can be concluded that the different behaviour of the effective Lewis number with respect to the standard one is due to the effective heat diffusion mechanism. It is observed that in [42] it was found that the effective heat diffusion time largely deviated from its standard quantity mainly for its mass diffusion contribution; although not checked here, this motivation is expected to be confirmed also in the present data.

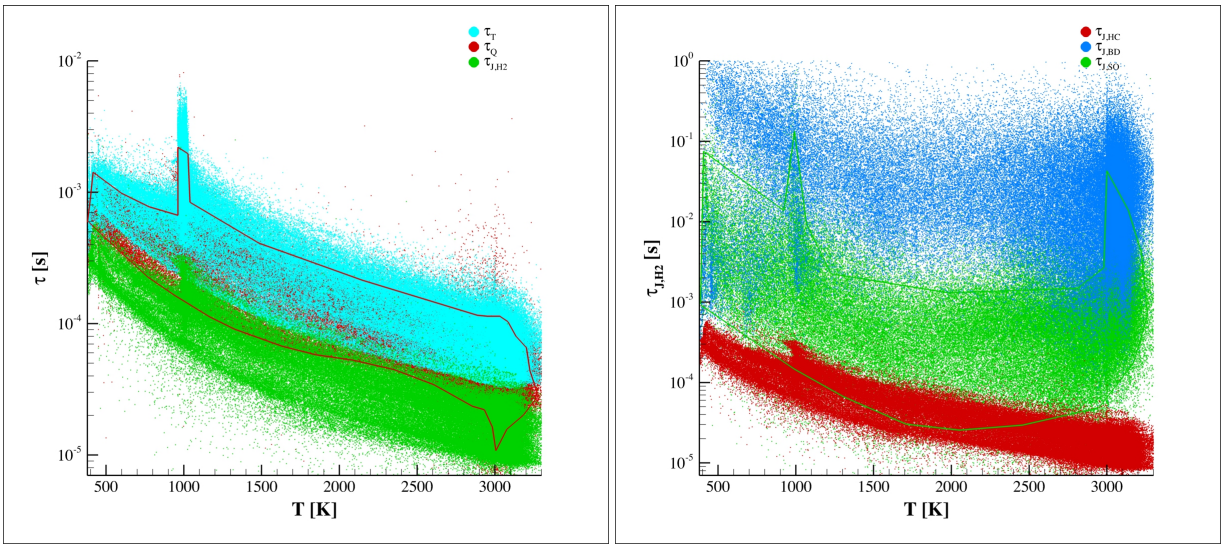

Figura 3.5: Case 90% O_2, $10^3 \times \kappa_P$. Instantaneous distributions of effective diffusive times (left): the edges of the heat diffusion time distribution are marked by a red line to help the reader. The associated Hirschfelder-Curtiss, baro-diffusion and Soret contributions to the hydrogen effective mass diffusion time are also shown (right): the edges of the Soret diffusion time distribution are marked by a green line.

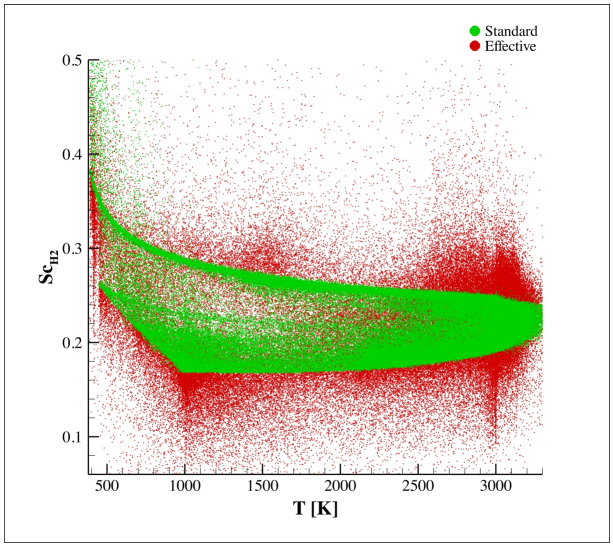

Figura 3.6: Case 90% O_2, $10^3 \times \kappa_P$. Instantaneous distributions of the standard and effective Schmidt numbers of hydrogen.

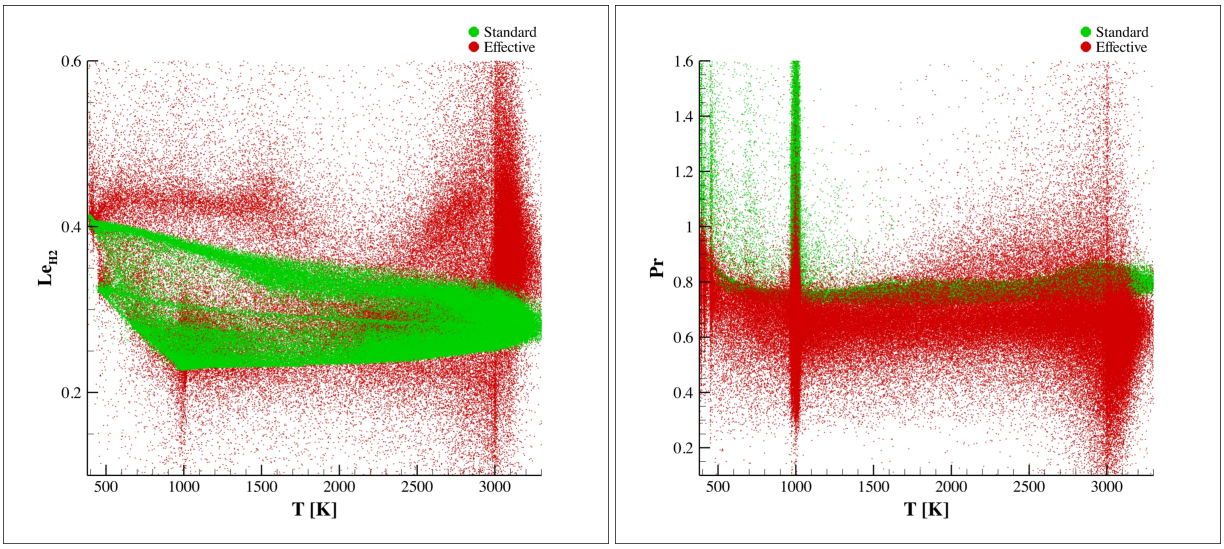

Figura 3.7: Case 90% O_2, $10^3 \times \kappa_P$. Instantaneous distributions of the standard and effective Lewis number of hydrogen (left) and of the Prandtl number (right).

4 Conclusions

The experience gained with the present real gas simulations proves the robustness of the numerical schemes implemented in the HeaRT code to simulate high-pressure oxy-combustion in s-CO_2 atmosphere.

Dilution effect of the oxygen stream by means of carbon dioxide was explored. Fixed the pilot flame imposed at the inlet between the reactant jets, it is found that dilution produce flame anchoring problems and not efficient combustion in the present shear-layer configuration. Hence, in the future attention should be focused on the design of injection strategies to enhance turbulent mixing at highly diluted O_2/CO_2 conditions.

The effect of radiant transfer of energy was taken into account by means of the M_1 diffusive model. Individual species' Planck mean absorption coefficients typically used at atmospheric pressure were assumed. Since they are expected to increase by increasing pressure, the effect of simply multiplying them by 1000 was investigated. In the future they will be accurately calculated by using high-resolution spectroscopic databases. It is observed that turbulence-radiation interaction is neglected for the time being, although it is expected to play an important role in flame cooling at the high-pressure conditions of the present simulations.

The chemical mechanism adopted in this work is too simple, it lacks of the main radical species and it is not validated at the extreme pressure conditions of the present numerical experiment. Hence, these simulations have to be considered as a first step before facing a more complex kinetics. The inclusion of radical species is expected not only to decrease the peak temperatures but also to affect ignition delay times and flame speed. Furthermore, the methane cracking reactions should be included in case of temperatures as high as those found in these simulations.

An original procedure already developed by the authors was adopted to estimate effective characteristic diffusion times. Effective characteristic numbers were also derived as ratio of effective times and compared to their standard counterparts. Conclusions already found in previous work by using different real gas flow simulations are here confirmed: the effective Prandtl and Lewis numbers differ from their standard counterparts. This may have strong implications in subgrid scale modelling of turbulent combustion in real gas flow simulations.

It is concluded that, upon the work done in this year and described in this report, the spatial numerical schemes ($AUSM^+ - up$ scheme coupled to a $WENO$ or $QUICK$ interpolation procedure) and the non-reflecting boundary conditions with their real gas extension, implemented in the HeaRT code, are robust enough to accurately simulate real gas turbulent mixing and combustion (excluding transcritical cryogenic liquid injection for the time being, due to less numerical stability exhibited). Hence, the ENEA in-house code HeaRT is now an advanced scientific instrument for numerical simulation in parallel computational frameworks. The next years will be focused on the identification of suitable injection and combustion strategies of reactants, to finally draw a "concept-design" of the $CH_4/O_2/s - CO_2$ injection plate and of the combustor of a $s - CO_2$ oxy-combustion cycle.

Acknowledgments

The computing resources and the related technical support used for this work have been provided by CRESCO/ENEAGRID High Performance Computing infrastructure and its staff [38]. CRESCO/ENEAGRID High Performance Computing infrastructure is funded by ENEA, the Italian National Agency for New Technologies, Energy and Sustainable Economic Development and by Italian and European research programmes (see http://www.cresco.enea.it/english for information).

Bibliografia

[1] E. Giacomazzi, D. Cecere, N. Arcidiacono, and F.R. Picchia. Schemi Numerici e Condizioni al Contorno Non Riflessive per la Simulazione di Gas Reali. Ricerca di Sistema Elettrico RdS/PAR2016/183, ENEA/MSE, September 2017.

[2] J.R. Howell, R. Siegel, and M.P. Menguc. *Thermal Radiation Heat Transfer*. CRC Press, Taylor & Francis Group, 5th edition, 2010.

[3] M.F. Modest and D.C. Haworth. *Radiative Heat Transfer in Turbulent Combustion Systems*. Springer Briefs in Applied Sciences and Technology. Springer, 2016.

[4] C. Caliot and G. Flamant. Pressurized Carbon Dioxide as Heat Transfer Fluid: Influence of Radiation on Turbulent Flow Characteristics in Pipe. *AIMS Energy*, 3(2):172–182, 2014.

[5] C.L. Tien. *Advances in Heat Transfer, Chpt. Thermal Radiation Properties of Gases*, volume 5. Academic Press, New York, 1968.

[6] H. Zhang and M.F. Modest. Evaluation of the Planck-Mean Absorption Coefficients from HITRAN and HITEMP Databases. *J. of Quantitative Spectroscopy and Radiative Transfer*, 73:649–653, 2002.

[7] L.S. et al. Rothman. The HITRAN 2008 Molecular Spectroscopic Database. *J. of Quantitative Spectroscopy and Radiative Transfer*, 110:533–572, 2009.

[8] L.S. Rothman, I.E. Gordon, R.J. Barber, H. Dothe, R.R. Gamache, A. Goldman, V.I. Perevalov, S.A. Tashkun, and Tennyson J. HITEMP, The High-Temperature Molecular Spectroscopic Database. *J. of Quantitative Spectroscopy and Radiative Transfer*, 111(15):2139–2150, 2010.

[9] L. Wang, D.C. Haworth, S.R. Turns, and M.F. Modest. Interactions Among Soot, Thermal Radiation, and NOx Emissions in Oxygen-Enriched Turbulent Nonpremixed Flames: a CFD Modeling Study. *Combustion and Flame*, 141(1-2):170–179, 2005.

[10] L. Wang, M.F. Modest, D.C. Haworth, and S.R. Turns. Modeling Nongray Soot and Gas-Phase Radiation in Luminous Turbulent Nonpremixed Jet Flames. *Combustion Theory and Modeling*, 9(3):479–498, 2005.

[11] J.B. Moss and C.D. Stewart. Spectrally Resolved Measurements of Radiative Heat Transfer in a Gas Turbine Combustor. *Experimental Thermal and Fluid Science*, 28(6):575–583, 2004.

[12] T. Ebara, N. Iki, S. Takahashi, and W.H. Park. Effect of Radiation Reabsorption on Laminar Burning Velocity of Methane Premixed Flame Containing with Steam and Carbon Dioxide. *JSME International Journal Series B - Fluids and Thermal Engineering*, 49(2):260–264, 2006.

[13] G.N. Mercer and R.O. Weber. Radiation Enhanced Combustion Wave Speeds. In *Proc. R. Soc. London A*, volume 453, pages 1543–1549. The Royal Society, 1997.

[14] S.R. Turns. *An Introduction to Combustion: Concepts and Applications*. McGraw-Hill, New York, 3rd edition, 2011.

[15] G.N. Minerbo. Maximum Entropy Eddington Factors. *Journal of Quantitative Spectroscopy and Radiative Transfer*, 20(6):541–545, 1978.

[16] D. Levermore. Relating Eddington Factors to Flux Limiters. *Journal of Quantitative Spectroscopy and Radiative Transfer*, 31:149–160, 1984.

[17] M. Anile, S. Pennisi, and M. Sammartino. A thermodynamical Approach to Eddington Factors. *Journal of Mathematical Physics*, 32, 1991.

[18] I Muller and T. Ruggeri. *Extended Thermodynamics*. Springer, 1993.

[19] J. Fort. Information-Theoretical Approach to Radiative Transfer. *Physics A*, 243:275–303, 1997.

[20] B. Dubroca and J.-L. Feugeas. *Etude Theorique et Numerique d'une Hierarchie de Modelles aux Moments pour le Transfert Radiatif*. C.R. Acad. Sci., 1999.

[21] T.A. Brunner and J.P. Holloway. One-Dimensional Riemann Solvers and the Maximum Entropy Closure. *Journal of Quantitative Spectroscopy and Radiative Transfer*, 69:543–566, 2001.

[22] J.-F. Ripoll, B. Dubroca, and G. Duffa. Modelling Radiative Mean Absorption Coefficients. *Combustion Theory and Modelling*, 5:261–275, 2001.

[23] J.-F. Ripoll. An Averaged Formulation of the M1 Radiation Model with Presumed Probability Density Functions for Turbulent Flows. *Journal of Quantitative Spectroscopy and Radiative Transfer*, 83:493–517, 2004.

[24] J.-F. Ripoll and H. Pitsch. Modelling Turbulence-Radiation Interactions for Large Sooting Turbulent Flames. In *Annual Research Briefs*, pages 41–52. Center for Turbulence Research, 2002.

[25] Giacomazzi E., Picchia F.R., and Arcidiacono N. A review on chemical diffusion, criticism and limits of simplified methods for diffusion coefficients calculation. *Combustion Theory and Modeling*, 12(1):135–158, 2008.

[26] Hirschfelder J.O., Curtiss C.F., Bird R.B., and Spotz E.L. *The Molecular Theory of Gases and Liquids*. John Wiley & Sons, New York, 1954.

[27] Babkovskaia N., Haugen N.E.L., and Brandeburg A. A high-order public domain code for direct numerical simulations of turbulent combustion. *Journal of Computational Physics*, 230:1–12, 2011.

[28] Bird R.B., Stewart W.E., and Lightfoot E.N. *Transport Phenomena*. John Wiley and Sons, New York, 2nd edition, 2002.

[29] Giovangigli V. *Multi-Component Flow Modeling*. Birkhauser, Boston, 1999.

[30] Rosner D.E. *Transport Processes in Chemically Reacting Flow Systems*. Dover, New York, 2000.

[31] Ern A. and Giovangigli V. Thermal diffusion effects in hydrogen - air and methane - air flames. *Combustion Theory and Modelling*, (2):349–372, 1998.

[32] de Charentenay J. and Ern A. Multicomponent transport impact on premixed turbulent H2/O2 flames. *Combustion Theory and Modelling*, 3(6):463–478, 2002.

[33] NIST (Agency of the US Department of Commerce). NIST Reference Fluid Thermodynamic and Transport Properties Database, http://webbook.nist.gov/chemistry/.

[34] Ern A. and Giovangigli V. EGlib: A general-purpose fortran library for multicomponent transport property evaluation. *Manual of EGlib version 3.4*, 12 July 2004.

[35] Andersen J., Rasmussen C.L., Giselsson T., and Glarborg P. Global combustion mechanisms for use in CFD modelling under oxy-fuel conditions. *Energy & Fuels*, 23:1379–1389, 2009.

[36] A. Frassoldati, A. Cuoci, T. Faravelli, E. Ranzi, C. Candusso, and D. Tolazzi. Simplified Kinetic Schemes for Oxy-Fuel Combustion. In *1st International Conference on Sustainable Fossil Fuels for Future Energy - S4FE*, Rome, Italy, 6-10 July 2009.

[37] Giacomazzi E., Cecere D., Picchia F.R., and Arcidiacono N. Sviluppo di un Modello LES per Fiamme Turbolente Premiscelate / Development of an LES model for turbulent premixed flames. PAR2013, Ricerca di Sistema, Accordo di Programma tra ENEA ed il Ministero dello Sviluppo Economico RdS/2013/255, ENEA (UTTEI-COMSO), Roma - Italy, October 2014.

[38] Ponti G. et al. The role of medium size facilities in the HPC ecosystem: the case of the new CRESCO4 cluster integrated in the ENEAGRID infrastructure. In *Proceedings of the 2014 International Conference on High Performance Computing and Simulation*, volume HPCS 2014, pages 1030–1033, 2014.

[39] M.S. Liou. A sequel to AUSM, part II: AUSM$^+$-up for All Speeds. *J. of Computational Physics*, 214:137–170, 2006.

[40] E. Giacomazzi, D. Cecere, N.M.S. Arcidiacono, G. Rossi, and F.R. Picchia. Les code development and validation. Technical Report WP4140b - CIRA-CF111310 V.1, CIRA - Italian Aerospace Research Center, November 2017. Project: Statement of Work for an Activity on Large Eddy Simulation for Application on LOx/CH4 Rocket Engines.

[41] E. Giacomazzi, D. Cecere, N.M.S. Arcidiacono, and F.R. Picchia. Approaching the Numerical Simulation of Trans- and Super- Critical Flows. In *8th European Combustion Meeting*, 18-21 April 2017. Dubrovnik, Croatia.

[42] E. Giacomazzi, D. Cecere, N.M.S. Arcidiacono, F.R. Picchia, G. Rossi, L. Cutrone, and A. Mastellone. Numerical Simulations of High-Pressure Mixing and Combustion'. In *AIAA Propulsion and Energy Forum*, number AIAA-2017-2707218. AIAA, 10-12 July. Atlanta, Georgia, USA.

[43] David H. Rudy and John C. Strikwerda. Boundary conditions for subsonic compressible Navier-Stokes calculations. *Computers & Fluids*, 9(3):327–338, sep 1981.

[44] Kevin W Thompson. Time-dependent boundary conditions for hyperbolic systems, II. *Journal of Computational Physics*, 89(2):439–461, aug 1990.

[45] Poinsot T.J. and Lele S.K. Boundary conditions for direct simulations of compressible viscous flows. *Journal of Computational Physics*, 101:104–129, 1992.

[46] M. Baum, T. Poinsot, and D. Thévenin. Accurate Boundary Conditions for Multicomponent Reactive Flows. *Journal of Computational Physics*, 116(2):247–261, feb 1995.

[47] Sutherland J.C. and Kennedy C.A. Improved boundary conditions for viscous, reacting, compressible flows. *Journal of Computational Physics*, 191:502–524, 2003.

[48] Nora Okong'o and Josette Bellan. Consistent Boundary Conditions for Multicomponent Real Gas Mixtures Based on Characteristic Waves. *Journal of Computational Physics*, 176(2):330–344, mar 2002.

[49] Polifke W. and Wall C. Non-reflecting boundary conditions for acoustic transfer matrix estimation with LES. In *Center for Turbulence Research Proceedings of Summer Program*, Summer 2002. Stanford.

[50] Klein M., Sadiki A., and Janicka J. A digital filter based generation of inflow data for spatially developing direct numerical or large eddy simulations. *J. of Computational Physics*, 186:652–665, 2003.

[51] P. et al. Strakey. Oxy-Combustion Flame Fundamentals for Supercritical CO2 Power Cycles. In *6th Interantional Symposium on Supercritical CO2 Power Cycles*, Pittsburgh, Pennsylvania, 27-29 March 2018.

[52] Nicolas Bouvet, Fabien Halter, Christian Chauveau, and Youngbin Yoon. On the effective lewis number formulations for lean hydrogen/hydrocarbon/air mixtures. *International Journal of Hydrogen Energy*, 38(14):5949 – 5960, 2013.

[53] Bruno Savard and Guillaume Blanquart. An a priori model for the effective species lewis numbers in premixed turbulent flames. *Combustion and Flame*, 161(6):1547 – 1557, 2014.

[54] K. Harstad and J. Bellan. The lewis number under supercritical conditions. *International Journal of Heat and Mass Transfer*, 42(6):961 – 970, 1999.